BIOCHEMISTRY
including biophysical chemistry & molecular biology

ARTICLE

pubs.acs.org/biochemistry

Effect of Glycerol and PVA on the Conformation of Photosystem I

Martin Hussels and Marc Brecht*

Universität Tübingen, IPTC, Auf der Morgenstelle 18, 72076 Tübingen, Germany

ABSTRACT: Single-molecule spectroscopy at cryogenic temperatures was used to examine the impact of buffer solution, glycerol/buffer mixtures (25% and 66%), and poly(vinyl alcohol) (PVA) films on the conformation of photosystem I (PSI) from *Thermosynechoccocus elongatus*. PSI holds a number of chromophores embedded at different places within the protein complex that show distinguishable fluorescence at low temperatures. The fluorescence emission from individual complexes shows inter- and intracomplex heterogeneity depending on the solution wherein PSI was dissolved. Statistical evaluation of spectra of a large number of complexes shows that the fluorescence emission of some of these chromophores can be used as sensors for their local nanoenvironment and some as probe for the conformation of the whole protein complex. Preparation in glycerol/buffer mixtures yields a high homogeneity for all chromophores, indicating a more compact protein conformation with less structural variability. In buffer solution a distinct heterogeneity of the chromophores is observed. PSI complexes in PVA show highly heterogeneous spectra as well as a remarkable blue shift of the fluorescence emission, indicating a destabilization of the protein complex. Photosystem I prepared in PVA cannot be considered fully functional, and conclusions drawn from experiments with PSI in PVA films are of questionable value.

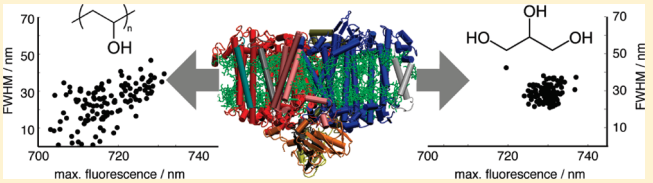

The proper functioning of proteins is a prerequisite for life. Beside intrinsic factors, the interaction of proteins with their surroundings is of high relevance, and a fundamental understanding of proteins must include extrinsic elements. System parameters like temperature, pressure, and pH value are important for the description of macroscopic system properties, but they fail in assisting us to describe proteins at the molecular level. A molecular description requires consideration of the protein moiety and the media wherein the protein is embedded. There, structure and dynamics of water close to the surface of proteins (hydration layer) are most important.[1,2] The properties of the hydration layer depend upon additives to the protein environment. Such additives can be small water-miscible organic solvents (cosolvents) or even huge chains of polymers. The remarkable effect of additives on protein function and their influence on the results of spectroscopic studies motivated experimental and theoretical groups to focus on the molecular details of their interaction with proteins.[3−12]

Here we focus on the influence of glycerol and PVA on the conformational properties of photosystem I(PSI). Glycerol is one of the most prominent cosolvents; due to its high biocompatibility, it is used in large amounts for cosmetics and pharmaceutics. Glycerol is also used as a protein stabilizer during crystallization[13] and as glass-forming agent for optical studies at low temperatures. The influence of glycerol on spectroscopic properties of proteins and their usability for the description of *in vivo* properties are examined by different experimental techniques[3,5,12] as well as by molecular dynamic simulations.[10,11] PVA is one of the most prominent water-soluble matrices; due to its excellent film forming, emulsifying, and adhesive properties, it is often used to immobilize proteins for experimental studies.[14] To gain a molecular picture of the polymer−protein interaction is challenging because the structural composition of the polymer and its variation due to changes of the environmental conditions like their water content must be addressed before the interaction with proteins can be approached.[15] On the basis of these restrains, a molecular picture for the interaction between these types of matrices and proteins is missing, and the influence of different types of matrices on the structure and function of proteins relies basically on phenomenological information.

Protein-embedded chromophores are native sensors for protein's conformation, which can be detected down to the single-molecule level. However, at room temperature the deduction of the conformational state and its dynamics is hampered by fast line broadening (spectral diffusion).[16−18] Lowering the temperature reduces the impact of fluctuations on the chromophores' site energies,[19,20] and the emission profile of a single emitter composed of a sharp zero-phonon-line (ZPL) and a phonon-wing (PW) becomes observable.[21−24] Single ZPLs can be observed if the rate of spectral diffusion is lower than the rate of acquiring spectrally resolved data as nicely shown by single-molecule spectroscopy (SMS) on LH2 at 1.4 K.[25] The width of those spectral jumps reaches into the range of several nanometers,[25,26] indicating remarkable changes in the site energy of the emitting molecules. However, in many cases the diffusion rate remains much larger than the acquisition rate, and only broadened lines are visible.[27,28]

Received: January 28, 2011
Revised: March 4, 2011
Published: April 15, 2011

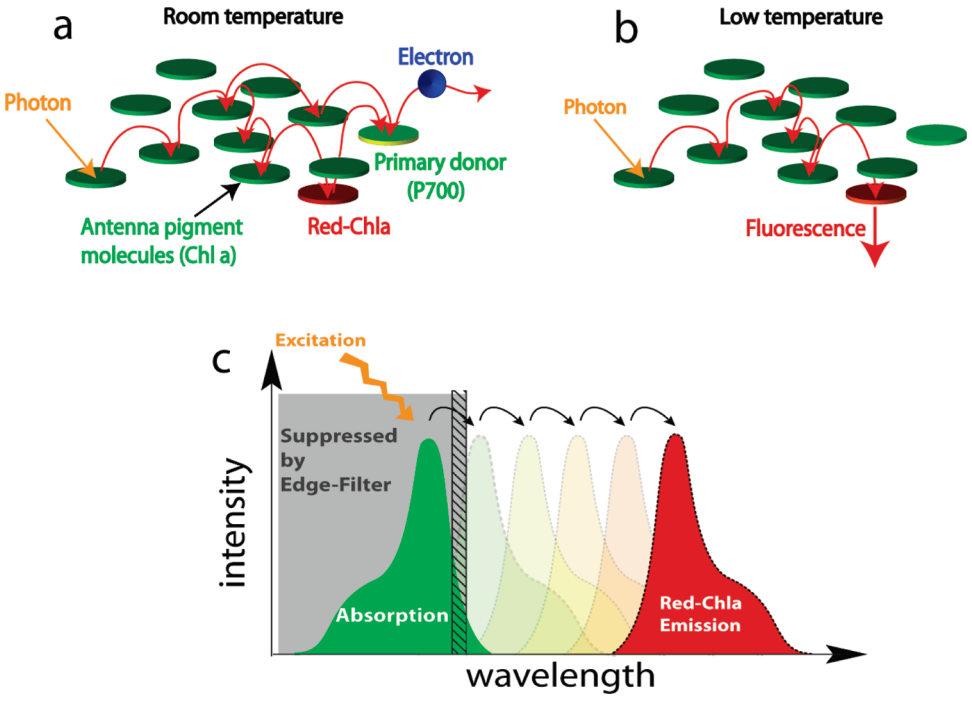

Figure 1. (a, b) Illustration of the excitation transfer within PSI at room and at low temperature. At room temperature, the initial excitation is transferred along energy transfer pathways until reaching P700 as indicated by red arrows. At low temperature the pathway from the red chlorophyll *a* molecules toward P700 is blocked. Next, the excitation is trapped in these states, and a large fraction of the initial energy is released by fluorescence emission. (c) The energetic arrangement of the different chromophores allows an effective excitation of the antenna system at the maximum of absorption. The large spectral separation of the maximum of absorption (green) and the fluorescence emission (dark red) ensures an efficient collection of the emission without restrictions by the edge filter (gray) used for blocking of stray light from the excitation source.

Here we study the fluorescence emission of single PSI complexes from cyanobacteria *Th. elongatus* dissolved in buffer solution, glycerol/buffer mixtures (25% and 66% (w/w)), and PVA films at cryogenic temperature (1.4 K). Over the past years we examined the fluorescence properties of single PSI complexes, and it turned out that PSI has preferential properties for general studies of protein dynamics at the single-molecule level.[29] The antenna system of PSI consists of ∼90 chlorophyll *a* molecules that form a very effective exciton transfer network.[30,31] This allows for efficient excitation of PSI at the absorption maximum (∼680 nm) far from the 700 nm absorption of the pigments P700, which is responsible for the primary photochemistry in PSI (see Figure 1).[32,33] A portion of the chlorophyll *a* molecules in the antenna system has site energies lower than 700 nm.[34] These low-energy pigments are often called the "red pools" or the "red-most" chlorophylls (for a review, see Gobets et al.[33] and Karapetyan et al.[32]). A very interesting property of PSI is its high quantum yield for charge separation upon exclusive low-energy excitation of its red pool chlorophyll *a* at ambient temperatures. The energy required for P700 activation is provided by thermal energy (see Figure 1a). At low temperatures the reduced thermal energy is insufficient for this process, and the low-energy chlorophyll *a* act as end points of the excitation transfer network. Under these conditions, the excitation energy is partially released as fluorescence light[35−37,34] with the maximum at wavelengths larger than 715 nm (see Figure 1b). This large red shift is very advantageous for SMS as the whole fluorescence emission of PSI composed of the several red pool emitters can be observed without interferences by the excitation light (see Figure 1c). The spectra of single PSI complexes show pronounced heterogeneities. In this article we use statistical analyses to correlate the observed heterogeneities with the properties of the solution/matrix wherein the PSI complexes are embedded.

MATERIAL AND METHODS

Preparation of Samples. PSI trimers from *Th. elongatus* have been isolated as described in ref 38. Then the purified PSI trimers were diluted in buffer solution (pH 7.5) containing 20 mM Tricine, 25 mM $MgCl_2$, and 0.4 mM β-DM as detergent to reach a chlorophyll *a* concentration of ∼20 μM. This amount of detergent is adequate for the critical solubilization concentration for a PSI trimer concentration of 0.5 μM to avoid PSI aggregation.[39] PSI samples in buffer solution were prepared adding 20 mM tricine, 25 mM $MgCl_2$, 4 mM β-DM, and 5 mM sodium ascorbate to Milli-Q water. Sodium ascorbate was added for prereduction of P700. The current mixtures were used to prepare PSI in glycerol/buffer and PVA/water mixtures instead of pure Milli-Q. In further steps the PSI-containing solution was diluted in buffer solution, buffer solution containing 25% glycerol (w/w), 66% glycerol (w/w), and 1% PVA (w/w). The final PSI trimer concentration was ∼3 pM. For PSI in buffer and glycerol/buffer less than 1 μL of these samples was placed between coverslips. For PSI in PVA 2 μL was spin-coated on a coverslip, and a second was placed on top. Sample preparation and mounting were accomplished under indirect daylight. Finally, the samples were transferred directly into the cryostat and rapidly plunged into liquid helium. Experiments were carried out using a home-built confocal microscope operating at 1.3−1.4 K. For the imaging of single molecules, a piezo tip tilt module (Physik Instrumente PI S-334.2SL) was used to deflect the beams. The excitation source was a diode laser (680 nm Schäfter

dx.doi.org/10.1021/bi2000615 |*Biochemistry* 2011, 50, 3628–3637

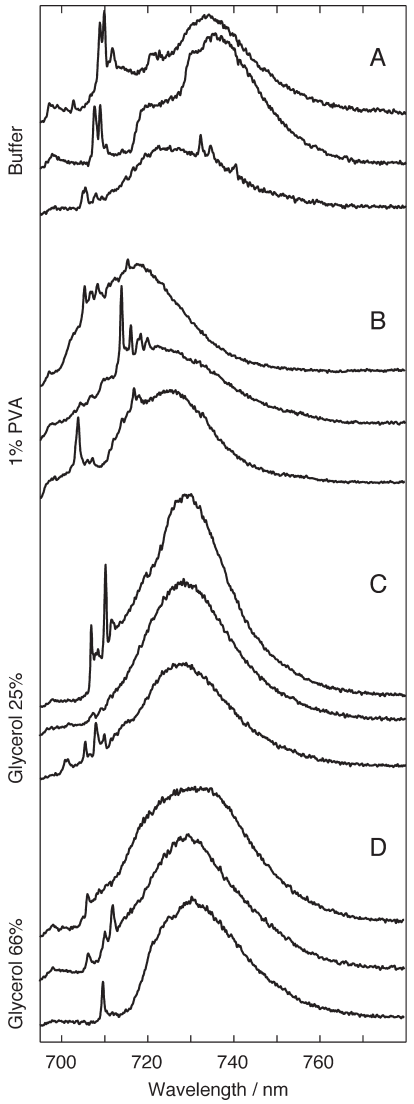

Figure 2. Fluorescence emission spectra obtained for single PSI complexes of *Th. elongatus* in different matrices. λ_{exc} = 680 nm, acquisition time 120 s, T = 1.4 K.

& Kirchhoff). The fluorescence emission was detected using either an avalanche photodiode (Perkin-Elmer SPCM-AQR-15, <50 dark counts/s) for fast integral fluorescence detection or an Acton Research 1/4 m spectrograph (Acton SpectraPro308) equipped with a back-illuminated CCD camera (Roper Scientific Spec-10:100BR/LN) for recording fluorescence spectra. Stray light of the laser was blocked by a Raman long-pass filter (AHF HQ695LP). For illumination and detection, the same microscope objective (60×, N.A. 0.8 JIS, Edmund Optics) was employed and immersed in liquid helium. A laser intensity of 100 μW, measured behind the scanning module, was used for excitation. In a sequence of spectra, the usual exposure time for each spectrum is 1 s, resulting in a typical S/N-Ration of >6 for single PSI complexes at the given excitation power referred as time resolution in the following context.

Data Evaluation Procedures. For data analysis we used two different types of algorithms named in the following algorithm I and algorithm II. For all evaluation the software package Matlab was used.

Algorithm I is used to determine the wavelength position of the fluorescence maximum and its full width at half-maximum (fwhm). From the series of fluorescence spectra from individual PSI trimers an interval containing the first 120 s is selected, and the average spectra are calculated, resulting in a S/N > 60; then a constant offset due to the CCD camera is subtracted, and the wavelength position of the most intense contribution is determined. Starting from the maximum position the width is determined where the intensity reaches the half of the maximum value. The wavelength position and the fwhm are collected for all spectra and given in a 2D representation as shown in Figure 3.

Algorithm II is used for the evaluation of ZPL occurrence in series of fluorescence spectra from individual PSI trimers. It is based on three steps. First, the spectra series are smoothed in two dimensions (wavelength and time) using a moving average filter as provided in Matlab (Curve Fitting Toolbox). In a second step, a standard Laplace 1D edge filter is applied in the wavelength domain to enhance sharp and to suppress broad structures. In a third step, all wavelength positions are collected where the intensity surpasses a certain threshold, which implies the presence of narrow lines in the spectra. Finally, the information is collected for all PSI complexes and visualized in histograms as given in Figure 6.

RESULTS

Fluorescence Emission Properties of Single PSI Complexes in Different Matrices. PSI complexes were prepared in buffer solution, glycerol/buffer mixtures with 25% and 66% (w/w) and PVA films. The concentration of PSI trimers was ~3 pM to ensure a spatial separation of individual PSI trimers much larger than the width of the focus of the excitation beam. In total, we recorded spectral information for 137 PSI complexes (trimers) in buffer solution, 108 in 25% glycerol/buffer mixture, 108 in 66% glycerol/buffer mixture, and 124 in a PVA film. Spectra of single PSI complexes of *Th. elongatus* taken in the different matrices are shown in Figure 2. There, three representative examples for spectra of single complexes are given for each matrix. The spectra have two different components: ZPLs and broad intensity distributions. ZPLs are found predominately in the wavelength range <720 nm, whereas the maxima of the broad intensity distributions are found in the wavelength range >720 nm. The emitters showing ZPLs are focused to spectral diffusion in the range of the setup's time resolution, whereas the emitters showing broad distributions diffuse much faster.[26,27]

Although the composition of the emission spectra is similar, a complex-to-complex variation of their shape is present. Nevertheless, a high similarity between the emission spectra is found in the glycerol/buffer mixtures. There, the wavelength position of the broad distributions undergoes slight changes, and only the width varies. In the case of the spectra taken in buffer solution and in PVA, the wavelength positions and the distribution width change. In glycerol/buffer mixtures the ZPLs are located in the region <715 nm, whereas for complexes in PVA films these lines can also be observed in the region around 720 nm and in buffer solution even in the far red region (up to 780 nm). The most red-shifted lines can be seen in the lower spectrum in Figure 2 for buffer solution, where lines are visible at 732, 734.5, and 740 nm. Aside from the line positions, their intensity shows remarkable variations. In spectra taken in buffer solution, the peak intensity of the ZPLs exceeds the intensity of the broad intensity distribution in some cases, whereas ZPLs found in the preparation with

glycerol/buffer never exceed the broad distribution and are generally of much lower intensity.

For better insight into the variation of the spectral shape present in different preparations, we used algorithm I (as described in the Material and Methods) to determine the wavelength position and the full width at half-maximum of the most intense contribution within the spectra regardless whether it is a ZPL or a broad distribution. These properties were determined and plotted for all spectra in 2D-scatter plots in Figure 3. This type of scatter plot serves as a helpful tool for the visualization of the heterogeneities present in different samples.[40] Scattering over wide wavelength and line width ranges is observed for buffer solution and PVA films; for the glycerol/buffer mixtures a reduced scattering is observed. The major proportion of spectra taken from PSI complexes in buffer solution show the most intense contribution within a wavelength range from 710 to 740 nm and the width varies between 15 and 40 nm. Besides this distribution, a number of contributions at around 710 nm are also present, showing very narrow line width. These contributions are due to the high intensity of the ZPLs sometimes exceeding the intensity of the broad intensity distributions as mentioned above. Such contributions were also found in the more red wavelength range around 733 nm.

The contributions found in the spectra taken on single complexes in PVA films also show a large scattering, and the whole distribution shows a blue shift. The span of the contributions found in PVA reaches from 703 to 730 nm for the wavelength positions and from 1 to 40 nm for the line width. Contributions at wavelengths >730 nm are rare, but a considerable number of contributions are observed at wavelength <710 nm.

Compared to buffer solution and PVA films, the spread of the contributions with the highest intensity found in glycerol/buffer mixtures is drastically reduced. This reduction is more pronounced for the wavelength positions of the contributions than for their line widths. For the 25% glycerol/buffer mixture, almost all contributions are found between 724 and 734 nm, and the width varies in the range of 22−38 nm. For the 25% glycerol/buffer mixture the uniformity of the spectra is more pronounced than for the 66% glycerol/buffer mixture: there more than 10 complexes also give rise to contributions outside of the compact region. Sharp lines with high intensity are not present over the whole wavelength region in glycerol/buffer preparation. Such lines remain features observed only in buffer solution and PVA films.

Average spectra obtained from summation of all investigated PSI complexes in the different matrices are shown in Figure 4. The maxima for the different preparations are found at 726.5 ± 0.5 nm (buffer solution), 730 ± 0.5 nm (glycerol/buffer mixtures 25%), 731 ± 0.5 nm (glycerol/buffer mixtures 66%), and 719 ± 1.0 nm (PVA films); see also Table 1. The shapes of the average spectra for PSI complexes in buffer solution and glycerol/buffer mixtures show great similarity. The shape of the average spectra for PSI complexes in PVA films deviates from the other average spectra. The slope on its blue side is larger than those of the other spectra, whereas the red tail again shows a similar shape.

Direct observation of spectral diffusion acting on chromophores becomes possible by reducing the accumulation time in combination with continuous recording of spectra. In Figure 5, cut-outs from two sequences of continuous recorded spectra of individual PSI complexes showing spectral diffusion of ZPLs are given. The cut-out given on the left shows sharp emission lines in the range ~707−710 nm. One line seems to vary between two

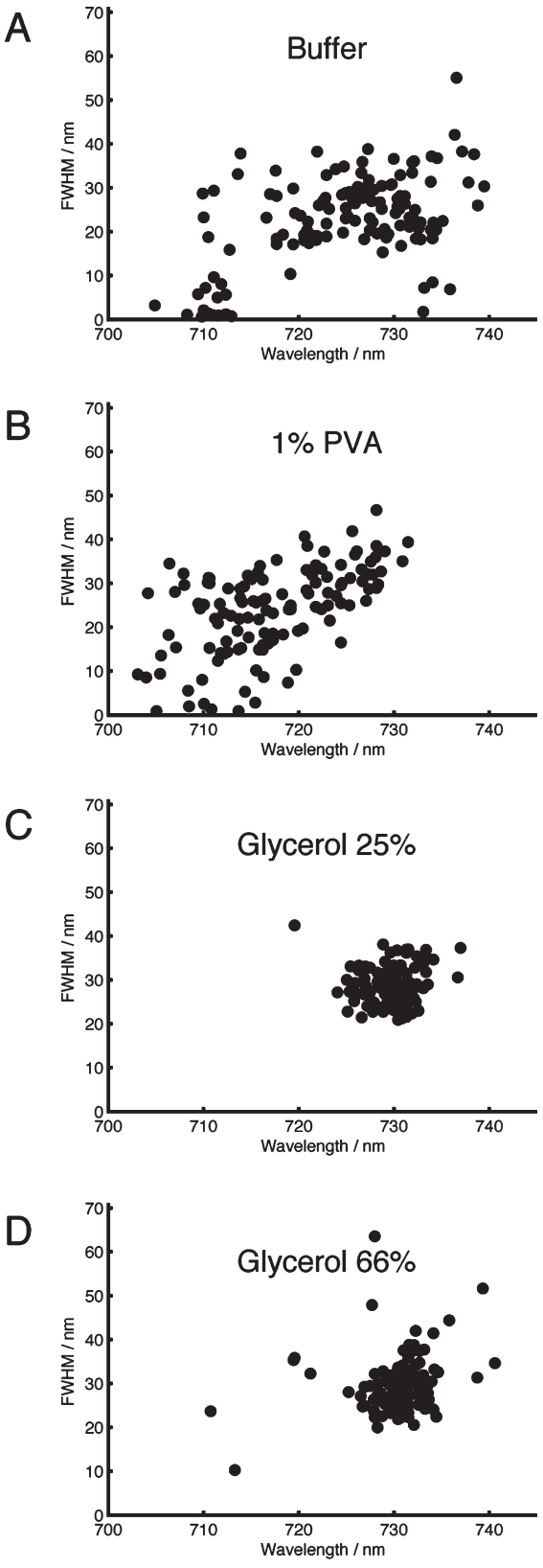

Figure 3. 2D-scatter plots obtained from the evaluation of the emission spectra from single PSI complexes in buffer solution (A), PVA (B), and glycerol/buffer mixtures of 25% (C) and 66% (D). Evaluation of the wavelength position and fwhm was done with algorithm I (for details see Material and Methods).

positions over time. The rate of spectral diffusion varies, but it remains mostly below the acquisition rate; therefore, one single line is observed in most spectra. More than one emitter contributes in the cut-out presented on the right. The emitter at ~710 nm changes its wavelength position only slightly during time. The largest jump of this line is observed after 43 s. The emission line beginning at 713.5 nm develops in a different way. After 15 s the line splits into two weaker lines. At t = 59 s these lines merge again to one stable line at ~717 nm.

Sequences of fluorescence spectra were recorded using the same experimental settings for all observed PSI complexes.

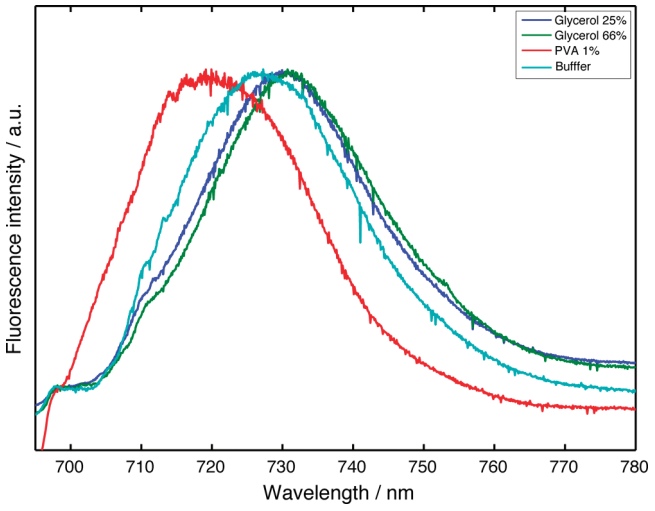

Figure 4. Averaged spectra obtained from the summation of 137 PSI complexes in buffer solution, 108 in 25% glycerol/buffer, 108 in 66% glycerol/buffer, and 124 in PVA film. Data were scaled to similar amplitude.

Algorithm II was used for the evaluation of the ZPL positions (as described in the Material and Methods). Algorithm II is specially designed to detect ZPLs in sequences of spectra. It accounts for their wavelength position, their time dependences, and occurrence. The intensity of the ZPLs is not object of the evaluation (like in the evaluation for the 2D-scatter plots in Figure 3). The data derived by algorithm II are given in Figure 6 together with their average spectra from Figure 4.

All histograms show the highest amount of ZPLs in the spectral region <720 nm; the maxima are found at around 710 nm (see Table 2). The widths of the distributions were determined by fitting with one Gaussian, they are: 3.1 nm for both glycerol/buffer mixtures, 4.1 nm for buffer solution, and 7.6 nm for PVA films. Sharp lines in the red wavelength range (>720 nm) are observed for around 30% of the complexes in buffer solution and 10% for PVA films, and for both glycerol/buffer mixtures almost no lines show up in the red region. The number of ZPLs detected within the sequence of spectra of one PSI complex are 1.6 in buffer solution, 3.0 in PVA films, and 1.2/1.1 for 25%/66% glycerol/buffer mixtures. The average widths of the ranges wherein algorithm II was able to determine the diffusion of the ZPLs are 1.1 nm in buffer solution, 1.4 nm in PVA films, and 1.0/0.9 nm for 25%/66% glycerol/buffer mixtures.

DISCUSSION

In this study we investigated the influence of buffer solution, glycerol/buffer mixtures, and PVA films on the optical properties of single PSI complexes at low temperatures.

First, we compare the spectral properties observed in our study with the results from ensemble experiments on PSI of *Th. elongatus*. Then, the capabilities of two evaluation methods are introduced, both of which could cope with the distinct spectral

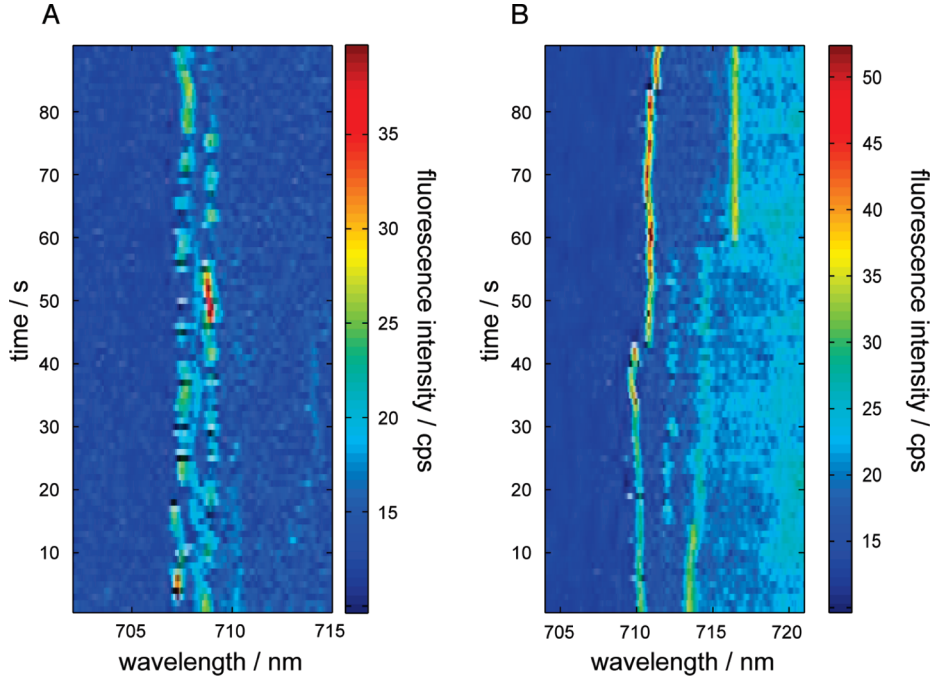

Figure 5. Time-dependent movement of ZPLs observed in the spectra of individual PSI complexes from *Th. elongatus*. Shown are 90 s cut-outs from time-dependent fluorescence emission spectra of two different complexes (A, B). The accumulation time for the individual spectra was 1 s; λ_{exc} = 680 nm; T = 1.4 K.

dx.doi.org/10.1021/bi2000615 |*Biochemistry* 2011, 50, 3628–3637

Table 1. Wavelength Position and Width of the Average Spectra Given in Figure 4 for the Different Preparations[a]

matrix	wavelength position/nm	width/nm
buffer	726.5 ± 0.5	31.8 ± 0.5
PVA 1%	719 ± 1.0	33.5 ± 0.5
glycerol 25%	730 ± 0.5	30.5 ± 0.5
glycerol 66%	731 ± 0.5	31.0 ± 0.5

[a] The error is due to the CCD camera calibration.

characteristics observed in the spectra of single PSI complexes. The results are related to structural changes of single chromophores or the whole protein complex. Finally, the molecular origin of the observed heterogeneity is considered.

Comparison of Single-Molecule and Ensemble Data. Optical measurements on PSI ensembles at low temperatures were only reported in glycerol/buffer mixtures; therefore, the comparison of ensemble and single-molecule data is restricted to this kind of preparation. The values of the fluorescence maximum in ensemble measurements were reported at 731 nm (70% w/v),[35] 730 nm (2:1 v/v),[37] and 732 nm (2:1).[41] The maxima of the fluorescence emission in glycerol/buffer mixtures found in the present study are at 730 nm (25%) and 731 nm (66%), in good agreement with the reported values.

In our study and in the study of Riley et al.[41] dissolved single crystals of PSI were used for the fluorescence measurements; therefore, the samples are similar. The comparison of the line shape of the average spectra shown in Figure 4 and the emission spectra of the ensemble (Figure 5 in ref 41) yields an almost perfect agreement. Therefore, we can conclude that the spectra derived at the single-molecule level are not biased, and the average spectra can be considered as ensemble-like data. This conclusion is advantageous, especially in the cases where no ensemble data are available, like for PSI in (frozen) buffer solution or PVA films (see Figure 4).

Evaluation of Heterogeneities in Single-Molecule Spectra of PSI. The spectra of single PSI complexes are composed of a number of contributions from different red pools.[26,29] The shape of these contributions vary between needlelike ZPLs and broad intensity distributions (see Figure 2). Sharp ZPLs are found predominately in the region below 720 nm; based on their low integral intensity, their contribution is almost invisible in the average spectra. These ZPLs are focused to spectral diffusion on the time scale of the actual time resolution of the setup (~1 s); hence, it is possible to follow their emission in time (spectral trails) as shown in Figure 5. The spectral range >720 nm is dominated by broad intensity distributions, and indications for stable emitting ZPLs are rare. The broad intensity distributions are due to emitters that are focused to spectral diffusion with high rates (≫1 Hz) and large spectral width (>10 nm).[27] In this case, the detection of ZPLs becomes impossible. The contributions to the fluorescence emission spectra of single PSI complexes differ in their number, intensity, and wavelength position. Therefore, it is impossible to draw conclusions on preparation related changes based on the comparison of a small number of those spectra.

To overcome restrictions induced by intercomplex heterogeneity, we applied statistical analyses to acquire reliable and comparable parameters. Two evaluation methods named algorithms I and II (see Material and Methods) were used for this purpose taking advantages of the spectral properties of PSI in different manner as pointed out in the following:

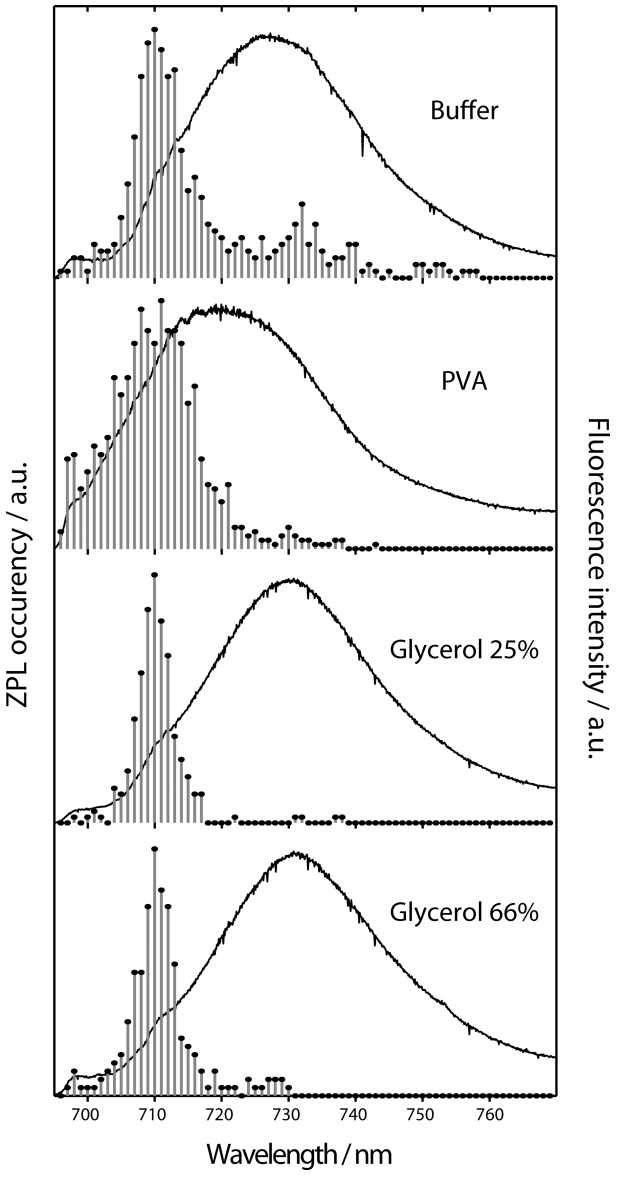

Figure 6. ZPL histograms for PSI complexes in buffer solution, glycerol/buffer 25%, glycerol/buffer 66%, and PVA film. The histograms result from algorithm II applied to time-dependent fluorescence emission spectra of single PSI complexes (for details see Material and Methods). In addition, the average spectra from the different preparations are given. The data were scaled to similar amplitude. Maximum positions and widths of the ZPL distributions are given in Table 2.

Algorithm I determines the wavelength position and width of most intense contribution in the spectra. The results for the different preparations are shown as 2D-scatter plots in Figure 3. The most intense contributions represent the end points in energy transfer within PSI, and their fluorescence intensity is a direct measure for the amount of excitation energy present. The excitation energy transfer from the initial point of photon absorption to the final trap involves a number of chlorophyll molecules distributed over the whole PSI complex. The heterogeneity of their site energies determines the heterogeneity of the energy transfer pathways. Therefore, the formation of energy transfer pathways depends sensitively on the structural heterogeneity of the whole complex. And vice versa, the most intense

contributions can be used as a measure for the structural heterogeneity of PSI.

Algorithm II determines the wavelength positions of narrow lines (ZPLs) in the spectra as shown in Figure 6. The major proportion of the ZPLs in PSI from *Th. elongatus* is centered around ~710 nm. They were assigned to chlorophylls, which absorb at 708 nm called C708.[35] The statistical analysis used in our previous studies was based on a manual determination of ZPLs and the wavelength range wherein the emission varies over time.[42] A manual evaluation is advantageous in some cases (which will be not discussed here), but the comparability of results is restricted. To overcome this drawback, we used algorithm II (see Material and Methods) for the determination of the ZPL positions with exactly the same filter parameters for all data sets. Using this approach, changes in the ZPL distributions for different preparation methods can be seriously considered. Observing changes in the shape of the ZPL distribution opens the possibility to draw conclusions about the subnanoscopic environments of C708.[24] Therefore, C708 can be used as a local probe within the PSI complex. In summary, the two evaluation methods are valuable to visualize changes of the overall structure of PSI and changes of one specific set of chlorophylls acting as a local probe.

Sample Heterogeneity in Buffer, Glycerol/Buffer, and PVA Films. The results from the four samples shown in the ZPL histograms (Figure 6), the 2D-scatter plots (Figure 3), and the average spectra (Figure 4) can be roughly divided into two groups: glycerol and non-glycerol containing samples. If glycerol is added, the samples show a distinct homogeneity; in the other cases (buffer solution and PVA) an increased heterogeneity is observed.

First, the findings for the glycerol containing samples are discussed. Their spectra are dominated by broad intensity distributions at >720 nm. The shapes of these distributions show only a small variation in bandwidth, and therefore, their contributions to the 2D-scatter plots form one well-defined cluster (see Figure 3c, d). The ZPL histograms show single Gaussian-shaped distributions with small width, and only very few complexes give rise to ZPLs at wavelength larger than 720 nm (see Figure 6). Nevertheless, in both representations it is notable that the homogeneity is slightly more expressed for the 25% than for the 66% mixture.

The observed effects in the glycerol/buffer mixtures are in agreement with the observed suppression of heterogeneity in protein samples by glycerol, where it is often added to enhance the crystallization of proteins.[13] It was considered that a protein will tend to minimize its surface in the presence of glycerol, which will lead to the stabilization of its structure.[11,43] This is in line with a lowered mobility of water within the hydration layer. The reduced mobility of water may act as a constraint on the accessible conformational space of the individual proteins yielding a homogenization of proteins.[10,12]

A glycerol induced suppression of the conformational flexibility of individual PSI complexes (intracomplex heterogeneity) as well as among different complexes (intercomplex heterogeneity) is observed. Furthermore, the suppression is observed for the structure of the whole complex (algorithm I) and for the environment of the local probe C708 (algorithm II). For the reaction center of *Heliobaterium chlorum* it was observed that the addition of glycerol has a distinct influence on the time constants of charge recombination.[44] Therefore, it remains an open question whether these homogeneous states induced by the addition of glycerol are representative for the native state of the protein or if they are just artificial states induced by glycerol.

Table 2. Wavelength Position and Width of the ZPLs Distribution Determined from the Data in Figure 6 by Fit with One Gaussian

matrix	center position (nm)	σ (nm)
buffer	710.4	4.1
PVA 1%	710.0	7.6
glycerol 25%	709.9	3.1
glycerol 66%	710.0	3.1

The group of the non-glycerol containing samples (buffer solution and PVA) shows some individual characteristics and are discussed individually. The preparation in buffer solution shows an increased spread of the contribution in 2D-scatter plot, indicating increased structural heterogeneity of PSI (see Figure 3a). Increased heterogeneity is also observed for the local probe C708; there, a broadening of the line width of the ZPL distribution compared to the glycerol/buffer mixtures is observed (see Figure 6). The average spectrum (see Figure 4) shows only minor indication of these changes; therefore, experiments at the single-molecule level are necessary to observe these properties. Reasons for the heterogeneity can be different mobility of water within the hydration layer or partial crystallization of the buffer solution during freezing. The low viscosity of water compared to glycerol mixtures might result in a larger conformational space accessible for the proteins under the given circumstances. The heterogeneity is partially maintained by the shock-freezing method used and becomes observable in the emission spectra at low temperatures. On the other hand, the freezing method is not able to vitrify the buffer solution completely and may induce the increased heterogeneity. It is probable that some water layers close to protein surface form a glassy state, but the freezing rates are too low for vitrifying bulk water. Therefore, the bulk water will be in a partially crystalline state inducing stress in its surrounding that may influence the PSI complexes.

An increased spread in the 2D-scatter plot is also observed for the PVA preparation (see Figure 3b). The mean value of the contributions is blue-shifted with respect to the other preparations. The blue-shift is also observed in the average spectra (see Figure 4 and Table 1). The ZPL histogram shows a distribution almost twice as broad as those observed for glycerol/buffer mixtures and buffer solution. Additionally, a large number of complexes show a remarkable fluorescence emission at <705 nm (see Figure 3b). This emission indicates the deactivation of higher lying chlorophyll states showing almost no emission in intact PSI. The modification of the structure of PSI by PVA interferes with the proper function of the whole complex. The increased heterogeneity of the protein might be due to a distortion of the water−protein interface introduced by the PVA chains. Zhang et al.[45] found by examining the water−protein interface that the hydration water network loosens up from the native to the molten globule states, and the protein gets locally more flexible with larger global plasticity and partial unfolding. This transition might be forced by PVA. A blue-shift induced by PVA was also reported for LH2; there also a denatured protein structure was considered.[46] The large distortions induced by PVA indicate that proteins prepared in PVA cannot be considered fully functional, and conclusions drawn from such experiments are of limited value.

Molecular Origin of Spectral Variations. The red emitters of PSI are most probable due to tightly interacting chlorophyll *a*

multimers (dimers and one trimer). Structural changes affect the site energy of such multimers. These changes can be roughly divided into two groups: changes affecting the site energy of the individual chromophores and changes affecting the coupling between the chromophores.

Structural changes affecting the site energy of chromophores can e.g. just rely on slight changes of the conformation of a nearby water molecule. These changes give rise to a detuning of the emission frequency ν_i of the chromophore. In the most simple approach a change of distance R between the water molecule and the chromophore is assumed. This change detunes the site energy of the chromophore by $\delta\nu_i$. Such dependencies can mostly be described by an equation $\delta\nu_i \sim n/R^{n+1}$.[47] Assuming a simple dipole−dipole interaction results in a shift of the transition energy given by $\delta\nu_i \sim |(-\mu_{water}\Delta\mu/2\pi\varepsilon hc)(1/R^3)|$ with ε being vacuum permittivity, h being Planck's constant, c equaling the speed of light, μ_{water} representing the dipole moment of water, and $\Delta\mu$ representing the difference of the static dipole moment between the excited and ground state of the chromophore. For a water molecule close to a chromophore, $\delta\nu_i$ can easily reach the nanometer scale.[19]

Structural changes affecting the coupling between chromophores rely on reorientations of the involved chromophores. Those reorientations can affect the interchromophore distance or their orientations. The strength of the coupling is described by the excitonic coupling $J_{ij} \sim (\vec{a}\cdot\vec{d} - 3(\vec{a}\cdot\vec{R})(\vec{d}\cdot\vec{R}))/R_{ij}^3$, with $\vec{a}$ and $\vec{d}$ being unit vectors in the directions of the acceptor and donor transition dipoles and $\vec{R}$ in the direction of the line joining the dipole centers.[31]

Both cases have in common that $\delta\nu_i$ and J_{ij} show a nonlinear dependence on distance R. Fluctuations of R by $\pm\Delta R$ have a much larger effect on $\delta\nu_i$ and J_{ij} if the coupling is already large. Consequently, an increase in the emission frequency caused by these mechanisms is accompanied by an increased spectral width induced by fluctuations. This correlation should result in a wavelength dependence of the inhomogeneous width. The discussed effect is visible in the 2D-scatter plot of the PVA preparation in Figure 3b. There, the contributions at low wavelengths show small widths and the red-most contributions show a larger width. This tendency is also visible for the preparation in buffer solution (Figure 3a), but there the tendency is covered by the reduced spectral diffusion observed in some complexes at higher wavelength. The spread of the data in the scatter plot for the preparation in glycerol/buffer mixtures is too small to evaluate this tendency.

The fluorescent states with clearly visible ZPLs show their emission maxima at ∼710 nm (see Table 2). This value is not seriously influenced by the different preparation methods. Only the spread of the distribution over the wavelength axis differs, indicating changes in the heterogeneity of the sample. The distribution of ZPLs with the lowest value of 3.1 nm is observed for the glycerol/buffer mixtures, whereas the width is increased to 7.6 nm for PVA. A stable emission wavelength accompanied by a change in line width was also observed for cytochrome c in trehalose film as compared to a glycerol/buffer mixture.[47] There, the line width of the $Q_x(0-0)$ transition is increased almost by a factor of 2 from glycerol/buffer to trehalose. Later it was shown by X-ray spectroscopy that the trehalose matrix perturbs the energy landscape of cytrochrome c, giving rise to well-resolved structural distortions close to the chromophore.[48] On the basis of these observations, it is reasonable that the nearby surrounding of the chromophores responsible for the emission at ∼710 nm undergoes structural distortions induced by PVA.[46] But a macroscopic rearrangement of the binding pocket can be excluded because the emission of C708 stems from chlorophyll a molecules that are red-shifted by almost 30 nm compared to chlorophyll a in solution. This red-shift is based on a highly balanced interaction between amino acid residues and chromophores in the binding pocket. Large rearrangements of the binding pocket will have drastic effect on the site energies of C708, and that is not in agreement with the data, which show a maintaining of the basic properties.

The emitters visible as broad intensity distributions show an even larger red-shift than C708. The large red-shift and spectral width covered by the diffusion process indicates the combination of a tight excitonic coupling of chromophores with high structural flexibility. The width of these distributions is maintained for the preparation in buffer and in glycerol/buffer mixtures. Some narrow lines can be observed in buffer solution, indicating lowered spectral diffusion, but their number is low. Changes induced by these preparation methods are unable to modify the properties of these chromophores seriously. Therefore, the structure of the binding pocket is not affected. The large width of the spectral diffusion is also maintained for PVA, but the center of the broad distributions and their spread are changed, as seen by a shift of up to 16 nm in the average spectra between PVA and 66% glycerol/buffer mixture (see Figure 4) and an increased scattering in the 2D-scatter plot (see Figure 3). Therefore, the structure of the chromophore assembly must have changed to decrease the value of the red-shift by more than 10 nm, but the basic properties are maintained as the emission is still remarkably red-shifted, and the spectral shape is still dominated by broad distributions indicative of high structural flexibility. Distortions must have taken place that changed the interaction between the chromophores, but the binding pocket is still able to bind the chromophores in a way that induces a large red-shift and allows a flexibility similar to other preparations.

In conclusion, the fluorescence spectra of single PSI complexes prepared in glycerol/buffer mixtures show small intra- and intercomplex heterogeneity, whereas the spectra taken in pure buffer and PVA are heterogeneous. Glycerol induces a more compact protein conformation with less structural variability, whereas PVA induces a destabilization of the protein complex.

AUTHOR INFORMATION

Corresponding Author

*E-mail: marc.brecht@uni-tuebingen.de. Phone: +49-7071-29-76239. Fax: +49-7071-29-5490.

Funding Sources

This work was supported by Heisenberg-Programm of the Deutsche Forschungsgemeinschaft DFG (BR 4102/1-1 and BR 4102/2-1).

ACKNOWLEDGMENT

We thank R. Bittl (FU Berlin) for his continuous support. We also thank Eberhard Schlodder for PSI samples and helpful discussions. Volker Radics and Jana Nieder are gratefully acknowledged for technical advice and assistance during the measurements.

ABBREVIATIONS

PSI, photosystem I; PVA, poly(vinyl alcohol); SMS, single molecule spectroscopy; ZPL, zero-phonon line; PW, phonon wing; FRET, Förster resonance energy transfer; C708, red pool of *Th. elongatus*.

REFERENCES

(1) Tarek, M., and Tobias, D. J. (1999) Environmental dependence of the dynamics of protein hydration water. *J. Am. Chem. Soc. 121*, 9740–9741.

(2) Nakagawa, H., and Kataoka, M. (2010) Percolation of hydration water as a control of protein dynamics. *J. Phys. Soc. Jpn. 79*, 083801.

(3) Back, J. F., Oakenfull, D., and Smith, M. B. (1979) Increased thermal-stability of proteins in the presence of sugars and polyols. *Biochemistry 18*, 5191–5196.

(4) Ansari, A., Jones, C. M., Henry, E. R., Hofrichter, J., and Eaton, W. A. (1992) The role of solvent viscosity in the dynamics of protein conformational-changes. *Science 256*, 1796–1798.

(5) Lakshmikanth, G. S., and Krishnamoorthy, G. (1999) Solvent-exposed tryptophans probe the dynamics at protein surfaces. *Biophys. J. 77*, 1100–1106.

(6) Timasheff, S. N. (2002) Protein-solvent preferential interactions, protein hydration, and the modulation of biochemical reactions by solvent components. *Proc. Natl. Acad. Sci. U.S.A. 99*, 9721–9726.

(7) Zou, Q., Bennion, B. J., Daggett, V., and Murphy, K. P. (2002) The molecular mechanism of stabilization of proteins by TMAO and its ability to counteract the effects of urea. *J. Am. Chem. Soc. 124*, 1192–1202.

(8) Zinober, R. C., Brockwell, D. J., Beddard, G. S., Blake, A. W., Olmsted, P. D., Radford, S. E., and Smith, D. A. (2002) Mechanically unfolding proteins: The effect of unfolding history and the supramolecular scaffold. *Protein Sci. 11*, 2759–2765.

(9) Fenimore, P. W., Frauenfelder, H., McMahon, B. H., and Young, R. D. (2004) Bulk-solvent and hydration-shell fluctuations, similar to alpha- and beta-fluctuations in glasses, control protein motions and functions. *Proc. Natl. Acad. Sci. U.S.A. 101*, 14408–14413.

(10) Liu, F. F., Ji, L., Zhang, L., Dong, X. Y., and Sun, Y. (2010) Molecular basis for polyol-induced protein stability revealed by molecular dynamics simulations. *J. Chem. Phys. 132*, 225103.

(11) Vagenende, V., Yap, M. G. S., and Trout, B. L. (2009) Mechanisms of protein stabilization and prevention of protein aggregation by glycerol. *Biochemistry 48*, 11084–11096.

(12) Malardier-Jugroot, C., Bowron, D. T., Soper, A. K., Johnson, M. E., and Head-Gordon, T. (2010) Structure and water dynamics of aqueous peptide solutions in the presence of co-solvents. *Phys. Chem. Chem. Phys. 12*, 382–392.

(13) Sousa, R. (1995) Use of glycerol, polyols and other protein structure stabilizing agents in protein crystallization. *Acta Crystallogr. D51*, 271–277.

(14) Zeng, J., Aigner, A., Czubayko, F., Kissel, T., Wendorff, J. H., and Greiner, A. (2005) Poly(vinyl alcohol) nanofibers by electrospinning as a protein delivery system and the retardation of enzyme release by additional polymer coatings. *Biomacromolecules 6*, 1484–1488.

(15) Raffaini, G., and Ganazzoli, F. (2006) Protein adsorption on the hydrophilic surface of a glassy polymer: a computer simulation study. *Phys. Chem. Chem. Phys. 8*, 2765–2772.

(16) Lu, H. P., and Xie, X. S. (1997) Single-molecule spectral fluctuations at room temperature. *Nature 385*, 143–146.

(17) Rutkauskas, D., Novoderezhkin, V., Cogdell, R. J., and van Grondelle, R. (2005) Fluorescence spectroscopy of conformational changes of single LH2 complexes. *Biophys. J. 88*, 422–435.

(18) Schleifenbaum, F., Blum, C., Subramaniam, V., and Meixner, A. J. (2009) Single-molecule spectral dynamics at room temperature. *Mol. Phys. 107*, 1923–1942.

(19) Shibata, Y., Ishikawa, H., Takahashi, S., and Morishima, I. (2001) Time-resolved hole-burning study on myoglobin: Fluctuation of restricted water within distal pocket. *Biophys. J. 80*, 1013–1023.

(20) Hofmann, C., Ketelaars, M., Matsushita, M., Michel, H., Aartsma, T. J., and Köhler, J. (2003) Single-molecule study of the electronic couplings in a circular array of molecules: Light-harvesting-2 complex from rhodospirillum molischianum. *Phys. Rev. Lett. 90*, 013004.

(21) Huang, K., and Rhys, A. (1950) Theory of light absorption and non-radiative transitions in f-centres. *Proc. R. Soc. London, Ser. A 204*, 406–423.

(22) Pullerits, T., Monshouwer, R., van Mourik, F., and van Grondelle, R. (1995) Temperature-dependence of electron-vibronic spectra of photosynthetic systems - computer-simulations and comparison with experiment. *Chem. Phys. 194*, 395–407.

(23) Renge, I. (2008) Impurity spectroscopy in glasses and disordered crystals: Inhomogeneous broadening and electron phonon coupling. *J. Lumin. 128*, 413–420.

(24) Ratsep, M., Pajusalu, M., and Freiberg, A. (2009) Wavelength-dependent electron-phonon coupling in impurity glasses. *Chem. Phys. Lett. 479*, 140–143.

(25) Hofmann, C., Aartsma, T. J., Michel, H., and Köhler, J. (2003) Direct observation of tiers in the energy landscape of a chromoprotein: A single-molecule study. *Proc. Natl. Acad. Sci. U.S.A. 100*, 15534–15538.

(26) Brecht, M., Studier, H., Elli, A. F., Jelezko, F., and Bittl, R. (2007) Assignment of red antenna states in photosystem I from Thermosynechoccocus elongatus by single-molecule spectroscopy. *Biochemistry 46*, 799–806.

(27) Brecht, M., Studier, H., Radics, V., Nieder, J. B., and Bittl, R. (2008) Spectral diffusion induced by proton dynamics in pigment—protein complexes. *J. Am. Chem. Soc. 130* (51), 17487–17493.

(28) Krause, S., Aramendia, P. F., Tauber, D., and von Borczyskowski, C. (2011) Freezing single molecule dynamics on interfaces and in polymers. *Phys. Chem. Chem. Phys. 13*, 1754–1761.

(29) Brecht, M. (2009) Spectroscopic characterization of photosystem I at the single-molecule level. *Mol. Phys. 107*, 1955–1974.

(30) Scholes, G. D., Jordanides, X. J., and Fleming, G. R. (2001) Adapting the Förster theory of energy transfer for modeling dynamics in aggregated molecular assemblies. *J. Phys. Chem. B 105*, 1640–1651.

(31) Byrdin, M., Jordan, P., Krauss, N., Fromme, P., Stehlik, D., and Schlodder, E. (2002) Light harvesting in photosystem I: Modeling based on the 2.5-Angstrom structure of photosystem I from Synechococcus elongatus. *Biophys. J. 83*, 433–457.

(32) Karapetyan, N. V., Schlodder, E., van Grondelle, R., and Dekker, J. P. (2007) in *Advances in Photosynthesis and Respiration* (Golbeck, J. H., Ed.) Vol. 24, Springer, Berlin.

(33) Gobets, B., and van Grondelle, R. (2001) Energy transfer and trapping in photosystem I. *Biochim. Biophys. Acta 1507*, 80–99.

(34) Schlodder, E., Shubin, V. V., El-Mohsnwy, E., Rogner, M., and Karapetyan, N. V. (2007) Steady-state and transient polarized absorption spectroscopy of photosystem I complexes from the cyanobacteria Arthrospira platensis and Thermosynechococcus elongatus. *Biochim. Biophys. Acta, Bioenerg. 1767* (6), 732–741.

(35) Palsson, L. O., Dekker, J. P., Schlodder, E., Monshouwer, R., and van Grondelle, R. (1996) Polarized site-selective fluorescence spectroscopy of the long-wavelength emitting chlorophylls in isolated photosystem I particles of Synechococcus elongatus. *Photosynth. Res. 48*, 239–246.

(36) Byrdin, M., Rimke, I., Schlodder, E., Stehlik, D., and Roelofs, T. A. (2000) Decay kinetics and quantum yields of fluorescence in photosystem I from Synechococcus elongatus with P700 in the reduced and oxidized state: Are the kinetics of excited state decay trap-limited or transfer-limited?. *Biophys. J. 79*, 992–1007.

(37) Zazubovich, V., Matsuzaki, S., Johnson, T. W., Hayes, J. M., Chitnis, P. R., and Small, G. J. (2002) Red antenna states of photosystem I from cyanobacterium Synechococcus elongatus: a spectral hole burning study. *Chem. Phys. 275*, 47–59.

(38) Fromme, P., and Witt, H. T. (1998) Improved isolation and crystallization of photosystem I for structural analysis. *Biochim. Biophys. Acta, Bioenerg. 1365*, 175–184.

(39) Müh, F., and Zouni, A. (2005) Extinction coefficients and critical solubilisation concentrations of photosystems I and II from Thermosynechococcus elongatus. *Biochim. Biophys. Acta, Bioenerg. 1708*, 219–228.

(40) Rutkauskas, D., Novoderezhkin, V., Gall, A., Olsen, J., Cogdell, R. J., Hunter, C. N., and van Grondelle, R. (2006) Spectral trends in the fluorescence of single bacterial light-harvesting complexes: Experiments and modified Redfield simulations. *Biophys. J. 90*, 2475–2485.

(41) Riley, K. J., Reinot, T., Jankowiak, R., Fromme, P., and Zazubovich, V. (2007) Red antenna states of photosystem I from

cyanobacteria Synechocystis PCC 6803 and Thermosynechococcus elongatus: Single-complex spectroscopy and spectral hole-burning study. *J. Phys. Chem. B 111*, 286–292.

(42) Brecht, M., Radics, V., Nieder, J. B., and Bittl, R. (2009) Protein dynamics-induced variation of excitation energy transfer pathways. *Proc. Natl. Acad. Sci. U.S.A. 106*, 11857–11861.

(43) Gekko, K., and Timasheff, S. N. (1981) Mechanism of protein stabilization by glycerol - preferential hydration in glycerol-water mixtures. *Biochemistry 20*, 4667–4676.

(44) Deinum, G., Kramer, H., Aartsma, T. J., Kleinherenbrink, F. A. M., and Amesz, J. (1991) Fluorescence quenching in Heliobacterium-chlorum by reaction centers in the charge separated state. *Biochim. Biophys. Acta 1058*, 339–344.

(45) Zhang, L. Y., Yang, Y., Kao, Y. T., Wang, L. J., and Zhong, D. P. (2009) Protein hydration dynamics and molecular mechanism of coupled water-protein fluctuations. *J. Am. Chem. Soc. 131*, 10677–10691.

(46) Freiberg, A., Timpmann, K., and Trinkunas, G. (2010) Spectral fine-tuning in excitonically coupled cyclic photosynthetic antennas. *Chem. Phys. Lett. 500*, 111–115.

(47) Ponkratov, V. V., Friedrich, J., and Vanderkooi, J. M. (2002) Solvent effects on conformational dynamics of proteins: Cytochrome c in a dried trehalose film. *J. Chem. Phys. 117*, 4594–4601.

(48) Giachini, L., Francia, F., Cordone, L., Boscherini, F., and Venturoli, G. (2007) Cytochrome c in a dry trehalose matrix: Structural dynamical effects probed by X-ray absorption spectroscopy. *Biophys. J. 92*, 1350–1360.